PAPER • OPEN ACCESS

Condensed ECM-based nanofilms on highly permeable PET membranes for robust cell-to-cell communications with improved optical clarity

To cite this article: Brian Choi *et al* 2021 *Biofabrication* **13** 045020

View the article online for updates and enhancements.

Biofabrication

CrossMark

PAPER

Condensed ECM-based nanofilms on highly permeable PET membranes for robust cell-to-cell communications with improved optical clarity

Brian Choi[1] ⓘ, Jeong-Won Choi[1] ⓘ, Hyungwon Jin, Hye-Rim Sim, Jung-Hoon Park, Tae-Eun Park[*] ⓘ and Joo H Kang[*] ⓘ

Department of Biomedical Engineering, College of Information and Biotechnology, Ulsan National Institute of Science and Technology (UNIST), UNIST gil 50, Ulju-gun, Ulsan 44919, Republic of Korea
[1] These authors contributed to this work equally.
[*] Authors to whom any correspondence should be addressed.

E-mail: tepark@unist.ac.kr and jookang@unist.ac.kr

Abstract

The properties of a semipermeable porous membrane, including pore size, pore density, and thickness, play a crucial role in creating a tissue interface in a microphysiological system (MPS) because it dictates multicellular interactions between different compartments. The small pore-sized membrane has been preferentially used in an MPS for stable cell adhesion and the formation of tissue barriers on the membrane. However, it limited the applicability of the MPS because of the hindered cell transmigration via sparse through-holes and the optical translucence caused by light scattering through pores. Thus, there remain unmet challenges to construct a compartmentalized MPS without those drawbacks. Here we report a submicrometer-thickness ($\sim$500 nm) fibrous extracellular matrix (ECM) film selectively condensed on a large pore-sized track-etched (TE) membrane (10 μm-pores) in an MPS device, which enables the generation of functional tissue barriers simultaneously achieving optical transparency, intercellular interactions, and transmigration of cells across the membrane. The condensed ECM fibers uniformly covering the surface and 10 μm-pores of the TE membrane permitted sufficient surface areas where a monolayer of the human induced pluripotent stem cell-derived brain endothelial cells is formed in the MPS device. The functional maturation of the blood–brain barrier (BBB) was proficiently achieved due to astrocytic endfeet sheathing the brain endothelial cells through 10 μm pores of the condensed-ECM-coated TE (cECMTE) membrane. We also demonstrated the extravasation of human metastatic breast tumor cells through the human BBB on the cECMTE membrane. Thus, the cECMTE membrane integrated with an MPS can be used as a versatile platform for studying various intercellular communications and migration, mimicking the physiological barriers of an organ compartment.

1. Introduction

Microphysiological systems (MPS) mimicking various organ compartments in the human body attracted considerable interest due to their prodigious potential to predict drug toxicity and efficacy that was elusive with conventional studies based on animal models or 2D cell culture methods [1, 2]. Many MPS devices consist of compartmentalized chambers separated by *in vitro* basement membranes, particularly to mimic the epithelial and endothelial tissues. The basement membrane is a thin sheet-like extracellular matrix (ECM) mainly composed of collagen type IV and laminin networks that underlie epithelial and endothelial cell layers, which play important roles in structural support, building a barrier between tissue compartments, and maintaining the cell phenotypes regulated by cell-ECM interactions. It actively

interacts with the cells in a bidirectional manner through the cell surface receptors to create functional homeostasis of a specific tissue [3]. To mimic the *in vivo* basement membrane in MPS, semipermeable polymer membranes have been popularly used due to their simplicity to fabricate and relatively strong mechanical property. The characteristic of the semipermeable porous membranes is critical in constructing MPS because it determines the physiological relevance, the permeability of biomolecules across the membranes, and optical transparency permitting versatile microscopic imaging. For the past decade, polydimethylsiloxane (PDMS) porous membranes have been widely employed, which are biocompatible and stretchable; however, due to its polymer network structure making it absorb small hydrophobic molecules [4], it became an unfavorable material for drug testing applications. Currently, chemically resistant commercial synthetic membranes, such as polyester (PE) and polycarbonate (PC) track-etched (TE) membranes [5], have been extensively used as substrates for tissue barriers, including blood–brain barrier (BBB) [6], kidney proximal tubule [7], and oviduct [8].

In selecting a commercial TE membrane for fabricating MPS, several parameters, such as pore size, pore density, and thickness, should be examined for each dedicated application. The use of TE membranes having large pores ($3 \sim 10\ \mu$m) allows the wider applications of MPS, including cell migration and cancer metastasis through endothelial cell barriers [5]. However, it may not be achievable to establish a specific tissue barrier characteristic on a porous membrane with a pore size larger than 3 μm due to the unique property of cells [9, 10]. For example, brain endothelial cells cannot form a distinct tissue barrier on a porous membrane with a pore size >3 μm because they readily migrate through the pores, which inhibits the development of MPS mimicking transendothelial migration of cancer cells through a brain endothelium layer [9]. On the other hand, the TE membranes with a pore size in a range of $0.4 \sim 2\ \mu$m can provide enough contact areas for generating functional tissue barriers in MPS [5]. Those membranes, however, limit the physical interactions between cell populations growing on either side of the membrane and hamper the modeling of cell transmigration through the membranes due to their small pore sizes [5]. In addition, the membranes with high pore density designed for robust paracrine communications are generally translucent due to the light scattering through the membranes [5]. Because of the limited repertoire of commercial TE membranes, it is still challenging to construct a porous membrane in MPS that simultaneously satisfies the needs described above.

To overcome these problems and replace synthetic polymer-based membranes, vitrified ECM membranes were developed to more precisely mimic the biophysical and biochemical properties of native basement membranes [11]. This approach was advantageous over the conventional membrane inserts because they closely replicate the basement membranes' structure and compositions. However, the vitrified ECM membrane with the manipulable thickness (20 μm) hindered efficient molecular transport across the membrane. In addition, the method reported for integrating the vitrified ECM membranes with the PDMS devices using PDMS precursors is not applicable to fabricating MPS with chemically inert thermoplastic materials, such as PC and polymethylmethacrylate (PMMA), because it involves chemical and plasma treatment that may lead to inactivation of inherent ECM properties.

This study reports a thermoplastic MPS device incorporating highly permeable TE membranes with a pore size of 10 μm where tissue-specific ECM molecules are condensed to form nanoscale monolayers that close the through-holes while mimicking the native basement membranes surrounding an organ compartment. Because of the adjustable thickness of the ECM nanofilms on the TE membranes (less than 1 μm), the molecular and cellular interactions between the cells cultured on the upper and lower sides of the membrane, respectively, are significantly facilitated. More importantly, the proposed approach permits the transmigration of cancer cells across the BBB endothelial monolayers, which is unachievable with the MPS fabricated with TE membranes of pore sizes around 1 μm. The improved optical clarity enabled by the larger pore size (10 μm) also allows us to visualize three-dimensional (3D) cell configuration more clearly, even across the condensed-ECM-coated TE (cECMTE) membrane using a confocal microscope.

2. Experimental section

2.1. Cell culture

Cytolight Green-expressing human umbilical vein endothelial cells (HUVECs; Sartorius) were cultured in complete endothelial cell medium (ECM; ScienCell) supplemented with endothelial cell growth supplement (ScienCell), 5% fetal bovine serum (FBS; ScienCell), and 1% penicillin/streptomycin (P/S; ScienCell) solution. Human lung adenocarcinoma cells (A549, ATCC® CCL-185™) were cultured in Ham's F12 medium (Welgene) containing 10% FBS and 1% P/S solution. Human primary astrocytes (Cat#1800; ScienCell) were maintained in Astrocyte Medium (ScienCell) and used at passage number 4. MCF-7 and MDA-MB-231 (KCLB) were maintained in RPMI1640 medium (Welgene) supplemented with 10% FBS and 1% P/S. Each cell was cultured at 37 °C and 5% CO_2 incubator (ICO105; Memmert). Each

medium was replaced every 2–3 d, and cells were sub-cultured or harvested when they reached around 80% confluency.

2.2. Human brain microvascular endothelial cell (hBMEC) culture and differentiation

The human induced pluripotent stem cell (iPSC) line (IMR90-4) was purchased from WiCell Research Institute and maintained on Matrigel (Corning) using TeSR™-E8™ (STEMCELL Technologies) according to WiCell Feeder Independent Pluripotent Stem Cell Protocols provided by the WiCell Research Institute (www.wicell.org). hBMECs were differentiated from iPSCs as previously described with minor modification [6]. To generate the hBMECs, IMR90-4 iPSCs were singularized using Accutase (Merck) and seeded on a 6-well plate coated with Matrigel at a density of 1.7×10^4 cells per well. Singularized cells were cultured with TeSR™-E8™ for 3 d until the concentration reaches 2.5×10^5 cells per well. To initiate differentiation (D0), the meddium was switched to the unconditioned medium (UM). UM is composed of 78.5% DMEM/F12 (Gibco), 20% Knockout™ Serum Replacement (Gibco), 1% non-essential amino acids (100×) (Gibco), 0.5% GlutaMAX™ supplement (Thermo Fisher Scientific), and 0.007% β-mercaptoethanol (Gibco). The culture medium was replaced every day by the fresh UM medium until D5. The endothelial cells were selectively expanded for 2 d (D6–D7) by switching to ECM, including human endothelial serum free medium (SFM) (Gibco) supplemented with 1% human serum (Sigma), 20 ng ml^{-1} bFGF (Peprotech), and 10 μM retinoic acid (Sigma). Cells were exposed to low oxygen tension (5% O_2, 5% CO_2) during differentiation (from D0 to D8) using a hypoxic chamber (Galaxy® 48 R; Eppendorf) [6].

2.3. Microfluidic device fabrication

Microfluidic channels were fabricated by engraving surface of PMMA substrates (width × height × depth; 10 cm × 5 cm × 1.5 mm) by a computer numerical control milling machine (David 3020C; David). Depending on experimental conditions and cell lines, different microchannel dimensions were used. The general width of microchannels was identical (width; 800 μm), in using HUVEC and A549 cell lines, the depths of microchannels were 200 μm. For hBMECs, deeper depths of 500 μm were used to expand the medium access. To improve optical transparency, milling marks on the microfluidic channel surface were removed by filling the inside of the PMMA microfluidic channels with 80% ethanol (Biosesang) and placing them in a convection oven at 100 °C (C-D0D1; Changshin Science) for 1 min. The microfluidic device was composed of two microchannels separated by a thin, porous polyester track-etched (PETE; SterliTech, it4ip) membrane, and it was fabricated as previously reported [12]. After the device fabrication, the microchannels were washed with isopropanol, ethanol, and deionized water sequentially. Then, the device was dried with nitrogen gas and kept in a sterile environment until the ECM coating process.

2.4. Condensed ECM coating

Collagen was used as the primary ECM coating solution. Various concentrations (2, 1, 0.125, 0.06 mg ml^{-1}) of rat tail collagen type I (Thermo Fisher Scientific) solutions were prepared through the manufacturer's protocols. The condensed ECM coating was achieved by injecting the prepared collagen solution into the microchannels of the device and performing the air-dry. During the process, to minimize the collagen sticking to the microchannel wall and ensure that the collagen was primarily coated on the porous TE membrane, each channel was blocked with the 3% bovine serum albumin (BSA; Sigma) solution for 1 h in an incubator (37 °C and 5% CO_2). The microchannels were then filled with the prepared collagen solution. Air bubbles trapped inside the microchannel were checked and removed through pipetting before the collagen gelation. The device was incubated at 37 °C for 2 h to complete the collagen gelation inside the microchannel, and it was moved to a sterile environment and dried overnight to condense the collagen to form an ECM nanofilm on the TE membrane.

2.5. Contact angle measurement

PMMA substrate and PETE membrane were coated with the BSA for 1 h in an incubator (37 °C and 5% CO_2). Water droplets dropped on each surface of the PMMA substrate and PETE membrane, and the contact angle of droplets was measured by the contact angle analyzer (Phoneix 300; Surface Electro Optics).

2.6. Scanning electron microscopy (SEM)

For SEM imaging, the cECMTE membrane samples were collected by disassembling the microfluidic device. The collected membrane was cut to a smaller size that includes the microchannel portion where the cECMTE membrane was formed. The samples were sputtered with platinum and mounted on the SEM microscope (S4800; Hitachi High Technologies). SEM images were taken to confirm the morphological characteristics of the cECMTE membrane. The obtained images were analyzed by ImageJ.

2.7. Microfluidic cell culture

To qualitatively compare the effect of the PETE membranes' pore size and porosity on the optical transparency, GFP-HUVEC was cultured in the upper channel spaces of the condensed ECM-coated microfluidic device, which integrated with different pore-size (1, 5, and 10 μm) PETE membranes.

The microfluidic channels were washed with $1\times$ phosphate-buffered saline (PBS; Biosesang) and filled with ECM, at least for 30 min for the ECM rehydration process. Then the culture medium with the suspended HUVEC (3×10^6 cells ml^{-1}) was injected into the upper microfluidic channel of the device and allowed the cells to attach to the PETE membrane surface under static conditions for at least 1 h. After the cell attachment was confirmed, the microfluidic device was connected to a syringe pump (Fusion 200; Chemyx Inc.), and the culture medium were infused through each channel at a flow rate of 2 μl min^{-1}. After 48 h, once cell monolayers were confluently established on the cECMTE membrane, cell images were visualized using a fluorescent microscope (EVOS® FL; Thermo Fisher Scientific). Each image was obtained by accepting emission light of the cell pass through the pores of the PETE membrane with an objective lens of the microscope.

To verify that cells were cultured within a specified compartment of the microfluidic device, GFP-HUVEC and A549 were cocultured in the upper and lower side of the cECMTE membrane of the device, respectively. GFP-HUVEC cells were seeded in the same process as described above. For seeding A549 cells, the microfluidic device was flipped, and A549 cells (5×10^6 cells ml^{-1}) suspended in the culture medium were injected into the lower microfluidic channel and allowed to attach to the lower side of the PETE membrane surface under a static condition for 1 h. After 48 h of cultivation with the syringe pump (2 μl min^{-1}), 5 μM solution of CellTrackerTM Red (Thermo Fisher Scientific) was loaded into the lower microchannel and then incubated (37 °C, 5% CO$_2$) for 30 min to stain the A549 cells. The microfluidic channel was then flushed with $1 \times$ PBS to clear the remaining dye solution. To visualize 3D rendered images of cell monolayers, the confocal microscope (LSM 980 Configuration 16 NLO; Carl Zeiss, USA) was used.

2.8. Optical properties of TE membranes

The aberrations due to the TE membranes were verified by directly measuring the point spread functions (PSFs) through the membranes. The same experimental geometry as in observation of cultured cells was replicated by using two different objective lenses for (a) illumination onto and (b) detection through the two different sides of the membranes. Rather than the cultured cells emitting fluorescence, an optical focus generated by the illumination objective was used as the emitting light source for PSF measurements. The illumination and detection objectives had numerical apertures (NA) of 0.5 and 0.3, respectively. As the illumination objective lens has a higher NA, an effective point source could be generated on the top surface of the TE membranes. The detection objective was then focused on the same layer to

observe the effective PSFs after light from the point source propagated through the membranes. For each membrane, ten PSFs were measured over random positions across the membrane surface and averaged to obtain the effective PSF. The structural similarity index (SSIM) values of each image were calculated by using MATLAB.

2.9. BBB reconstruction in MPS device

For culturing hBMECs on a microfluidic device, an overall condensed ECM coating process was employed as described above except for the concentration of collagen type I (0.125 mg ml^{-1}). The microchannels pre-coated with the condensed ECM (collagen type I) were additionally coated with the mixture of 400 μg ml^{-1} collagen type IV (Sigma) and 100 μg ml^{-1} human fibronectin (Sigma). After overnight incubation at 37 °C, the microchannels were dried at room temperature for 20 min, followed by aspiration of coating solutions and rehydrating the channel using EC medium. For the co-culture of astrocytes and hBMECs, human astrocytes (1×10^6 cells ml^{-1}) were seeded on the lower side of the cECMTE membrane of the channel. The device was flipped and incubated for 2 h to allow the astrocytes to completely attach to the lower side of the membrane. After the astrocytes were stably attached, both channels were flushed with EC medium, and hBMECs were seeded with a density of 1.2×10^7 cells ml^{-1} on the upper side of the cECMTE membrane. After 6 h of seeding hBMECs, the EC medium was carefully exchanged through inlet and outlet holes to avoid nutritional deficiencies and dryness of the cells. The device was maintained at 37 °C in a 5% CO$_2$ incubator for 24 h and fed with the fresh EC medium deprived of bFGF and retinoic acid. All follow-up assays were carried out after 2 d of culture.

2.10. Immunofluorescence imaging

On the third day of hBMECs and astrocytes seeding on the device, cells were fixed for 15 min at room temperature by flushing 4% paraformaldehyde (Biosaesang) and permeabilized with 0.1% Triton X-100 (Sigma) in Dulbecco's phosphate buffered saline (DPBS) for 10 min. After blocking the cells with 10% goat serum diluted in PBS containing 0.1% Triton X-100 for 1 h at room temperature, samples in a microfluidic channel were treated with primary antibodies and incubated at 4 °C overnight. After the washing procedure, secondary antibodies were treated for 1 h at room temperature. Primary antibodies used in this study are listed in table S1 (available online at stacks.iop.org/BF/13/045020/mmedia). The secondary antibodies fluorescently conjugated with Alexa Fluor-488, Alexa Fluor-594, or Alexa Fluor-647 were used with 1:200 dilution when the primary antibodies are not conjugated. Nuclei were counterstained

with 4′,6-diamidino-2-phenylindole (DAPI;Sigma). Fluorescence images of cells were obtained using fluorescence microscopy (Nikon), confocal microscopy LSM780NLO (Zeiss), and LS980 (Zeiss).

2.11. qRT-PCR
Total RNA of hBMECs within a microchannel was extracted on the third day of seeding using a AccuPrep® Universal RNA Extraction Kit (Bioneer) and reverse-transcribed into cDNA using AccuPower® RT PreMix & Master Mix (Bioneer) in a thermal cycler (T100 Thermal Cycler; Bio-Rad). The quantitative real-time PCR was carried out using SYBR® Green Realtime PCR Master Mix (TOYOBO) on a CFX Connect Real-Time PCR Detection System (Bio-Rad). Table S2 shows the primer sequences used for real-time PCR.

2.12. Permeability assay
To measure the barrier function of the BBB, the BBB in an MPS device incorporating a 10 μm-pore cECMTE membrane additionally coated with BBB ECM (collagen IV and fibronectin) was used. The BBB on the 1 μm-pore PETE membrane coated with the BBB ECM were used as a control. On D10, 100 μg ml^{-1} of Lucifer yellow (Invitrogen) was applied to the upper channel (blood side) while the lower channel (brain side) was blocked. After 1 h of incubation, the medium from the brain side was carefully collected. The fluorescence of the samples was analyzed at 420/540 nm using a microplate reader (SynergeNeo2; Biotek). Apparent permeability is calculated according to the following formula:

$$P_{\text{app}} = \frac{C_x}{C_0 \times t(\text{s}) \times A(\text{cm}^2)} \times V(\text{ml}). \quad (1)$$

C_0 is the applied concentration and C_x is a measured concentration of the collected sample at time t. A is the area of the membrane within the channel, and V is the volume of the brain side channel, which is 0.16 cm^2 and 0.008 ml, respectively, in our device.

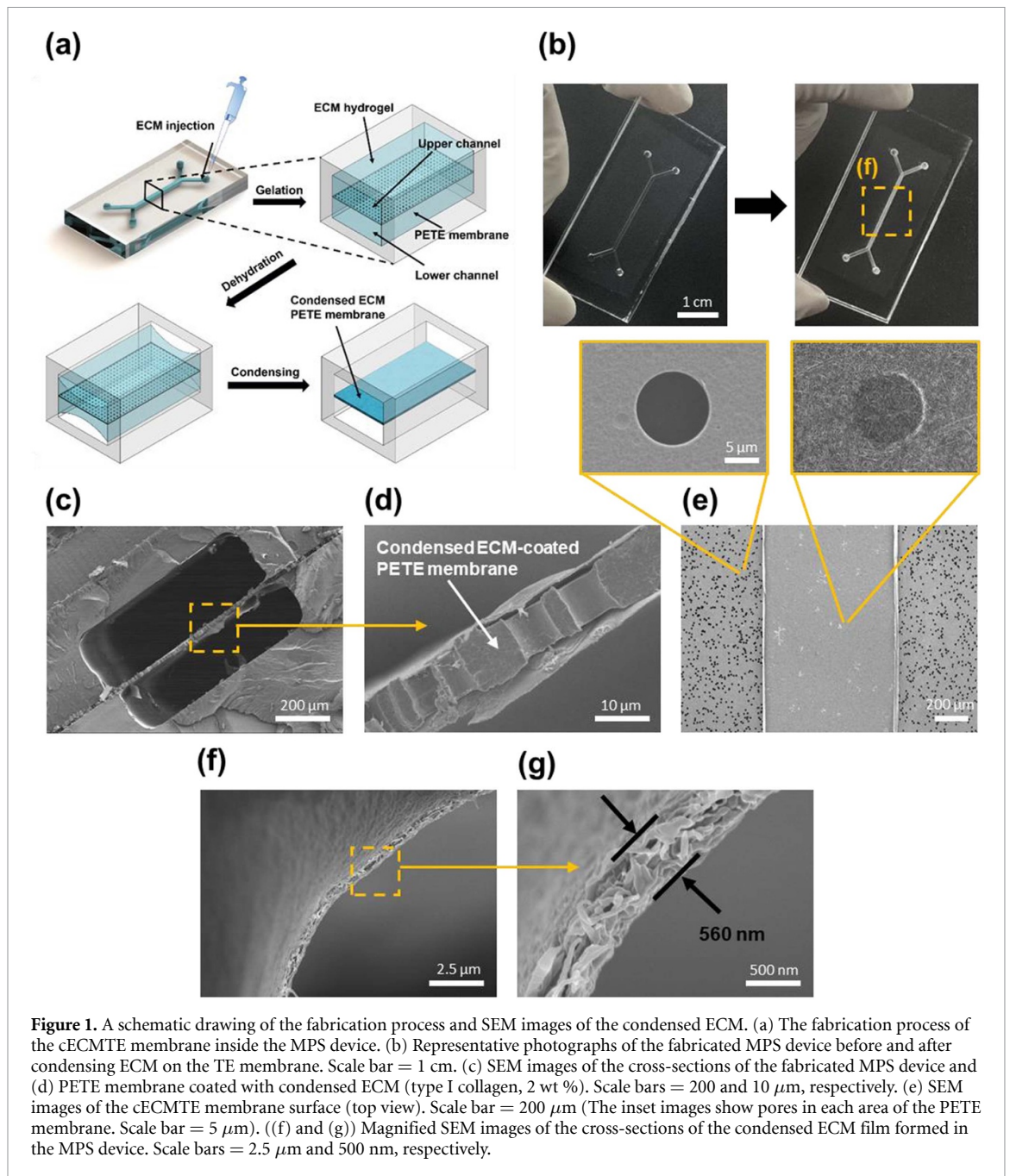### 2.13. Cancer cell transendothelial migration assay
Two types of human breast cancer cell lines, MCF-7 and MDA-MB-231, were labeled with CellTracker Green by incubating for 20 min at 37 °C. Followed by three times of washing, the labeled cancer cells were introduced to the upper channel of the BBB MPS (blood side) with a density of 3 × 10^6 cell ml^{-1}. After coculturing for 24 h, the devices were washed with DPBS to remove unattached cancer cells. To indicate the BBB layer, hBMECs were stained with ZO-1 antibody as described in the experimental section. In the device, the cells in transmigration steps were counted by taking an image of the entire microfluidic channel. The transmigrated and non-transmigrated cells were clearly distinguished in z-stack images under observation with the confocal microscope LSM980 (Zeiss).

3. Results and discussion

3.1. Fabrication of the cECMTE membrane integrated with an MPS
The ECM hydrogel is a porous and biocompatible material consisting of a 3D hydrophilic network of cross-linked polymers [13]. As the primary structural protein of the ECM, collagen forms the hierarchical network of fibrils much like the native tissue and acts as scaffolds for tissue engineering [14]. The temperature-responsive gelation of type I collagen can primarily provide the fibrillate network and has already been extensively studied [15, 16]. As mentioned, there were attempts to create a vitrified ECM membrane with the inspiration of collagen's characteristics as a structural protein [11, 17–19]. However, since those membranes were fabricated by a sequential process of gelation and dehydration of the ECM proteins, there were no support fixtures embedded in the membrane, and it was wrinkle-prone and had limited mechanical properties. Also, it was challenging to integrate that membrane with synthetic polymer devices since any chemical glue or plasma treatment was not available with the native ECM protein membrane. Based on this consideration, we combined the ECM membrane on the premanufactured polymeric base membrane to easily produce a synthetic polymer MPS device advancing the tissue engineering study in a microscale regime.

We formed the fibril network that surrounds the pre-integrated hydrophilic porous PETE membrane in the PMMA MPS device using type I collagen. Microchannels of a microfluidic MPS device were used as a mold system to condense the injected collagen solutions onto the PETE membrane to form nanoscale monolayers that mimic the native basement membrane (figure 1(a)). Depending on the microchannel volume, a certain amount of collagen was uniformly introduced into the microfluidic channels, and thermal gelation proceeded at 37 °C. After the collagen was firmly gelated, the water inside the collagen hydrogel evaporated by air-drying. Consequently, the volume of the hydrogel highly reduced, resulting in the condensed fibril network of collagen fibers, which also led to forming robust mechanical strength. During the condensation process, the nanofilm structure of the collagen fibers adhered tightly on both the upper and lower surface of the PETE membrane without any toxic chemical glue or plasma bonding (figure 1(a)). Before introducing the collagen, the microchannels were blocked with BSA to prevent the collagen matrix from being adsorbed onto the channel wall surface. Despite the BSA coating on the PETE membrane and the PMMA channel surface, the collagen fibers were still preferentially condensed on the PETE membrane rather than the PMMA channel surface due to the higher surface energy of the PETE membranes than the PMMA

Figure 1. A schematic drawing of the fabrication process and SEM images of the condensed ECM. (a) The fabrication process of the cECMTE membrane inside the MPS device. (b) Representative photographs of the fabricated MPS device before and after condensing ECM on the TE membrane. Scale bar = 1 cm. (c) SEM images of the cross-sections of the fabricated MPS device and (d) PETE membrane coated with condensed ECM (type I collagen, 2 wt %). Scale bars = 200 and 10 μm, respectively. (e) SEM images of the cECMTE membrane surface (top view). Scale bar = 200 μm (The inset images show pores in each area of the PETE membrane. Scale bar = 5 μm). ((f) and (g)) Magnified SEM images of the cross-sections of the condensed ECM film formed in the MPS device. Scale bars = 2.5 μm and 500 nm, respectively.

channel surface. The contact angles measured on the surface of a PMMA substrate and a PETE membrane, each of which was coated with BSA, were 10.05 ± 0.26° and 0°, respectively (figure S1). This supports that the higher surface energy of the PETE membrane than the PMMA substrates allowed the ECM solution to selectively condense onto the PETE membrane rather than onto the PMMA channel surface. Figure 1(b) represents photographs of the MPS devices before (left panel) and after (right panel) the condensed ECM coating process. After the coating, we observed that the channel part turned optically opaque, which indirectly confirmed the formation of the fibril matrix with the naked eye. However, the

cECMTE membrane returned to a transparent state once priming the channel with a culture medium to rehydrate the membrane.

Next, we directly observed the cECMTE membranes' surface morphology and nanofibrous structure using SEM images (figures 1(c)–(g)). Figure 1(c) shows a cross-sectional image of the MPS device containing the cECMTE membrane. A 10 μm-pore PETE membrane was located in between the upper and lower channels. A magnified view of the PETE membrane verified the presence of the condensed ECM nanofilm adhered on both the upper and lower sides of the membrane (figure 1(d)). On the surface of the PETE membrane disassembled from

the channel, distinctively visible condensed collagen fibers evenly covered the microchannel area of the porous membrane (figure 1(e), right inset panel). In contrast, the rest of the area remained without being coated with condensed ECM (figure 1(e), left inset panel). A magnified image of the 10 μm-pore membrane showed that randomly oriented collagen fibers were densely packed to organize the gapless mesh structure and closed the pore (figure 1(e), right inset panel). The structure or the porosity of the fibrillated collagen mesh was also adjustable by changing a collagen concentration. We condensed a range of concentrations of type I collagen (0.06, 0.125, 1, and 2 mg ml^{-1}) onto the 10 μm-pore PETE membranes in the MPS device and found that the minimal collagen concentration required for covering the pores without voids should be in a range between 0.125 and 1 mg ml^{-1} (figure S2). Figures 1(f) and (g) shows the representative cross-sectional images of the condensed ECM in a nanofilm structure. The thickness of the film was around 500 nm when 2 mg ml^{-1} of collagen was used. It was adjustable in several ways; by changing the concentration of the collagen solution, modifying the channel dimension to vary the volume of the collagen solution introduced into the microchannel, and continuously overlaying the condensed ECM on the same membrane. These SEM images of the ECM nanofilms revealed the morphology of the densely packed multilayered collagen fibers that mimic the native ECM nanofiber structure, and these morphological characteristics permitted robust mechanical property of the ECM membrane and more abundant opportunities for cells to interact with the surrounding microenvironment in comparison to a solution-based ECM coating method.

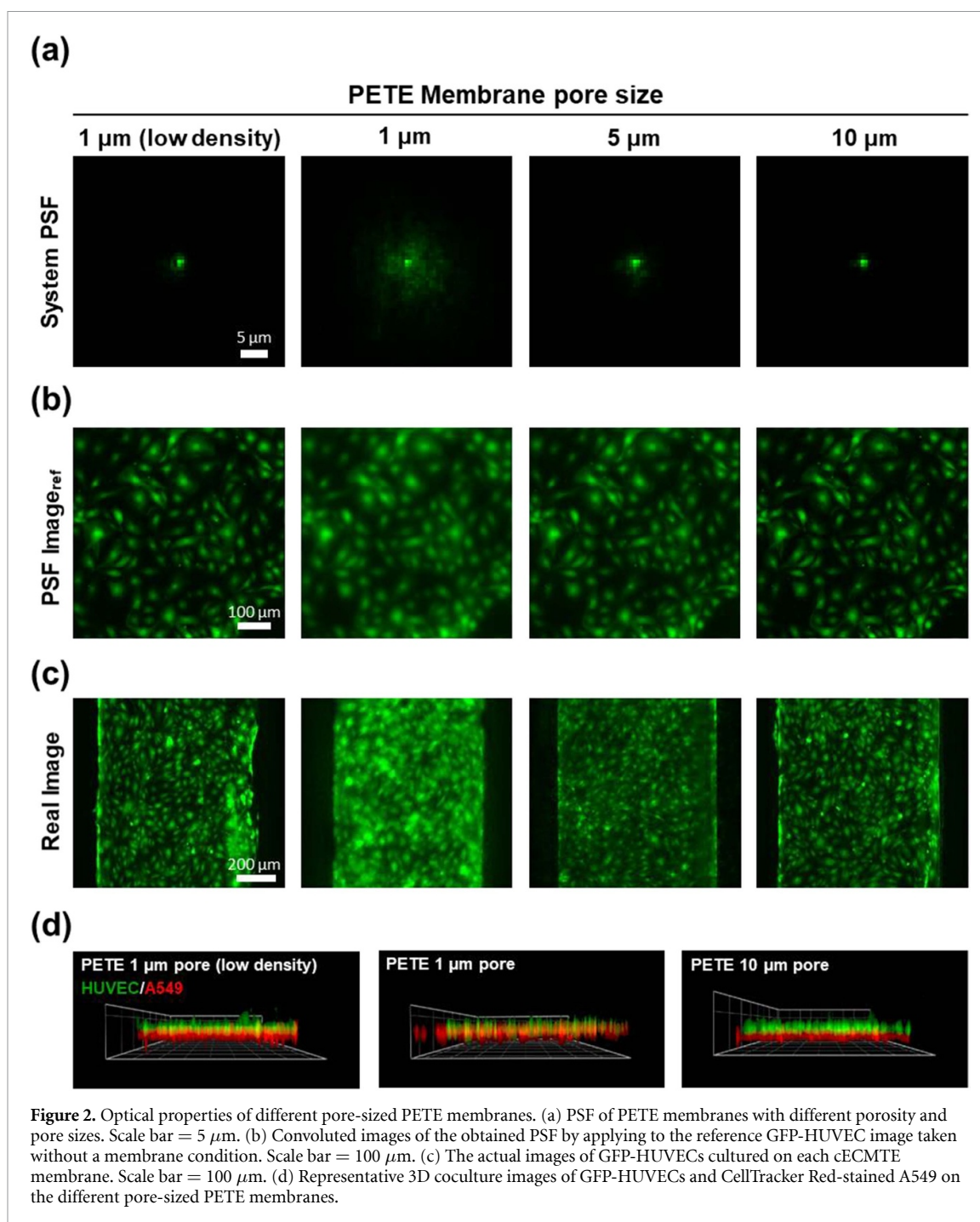### 3.2. Optical properties of porous PETE membranes

To construct the MPS, the optical properties of the membrane to accurately profile live cells are important [20]. Synthetic TE membranes are commercially available with a variety of options of pore sizes and densities. Those porous membranes allow light transmission through the surface to visualize cells on each side of the membrane. However, the transmitted light onto the membrane is scattered due to spacing between pores or its perforated angle, and it often generates some background signals, making images blurry and limit the application of the membrane [5]. In general, the membranes with lower pore density appear to have lower background signal. As the membrane with large pores does not allow uniform cell seeding, small pore-sized membranes (0.4 $\sim$ 2 μm) with low porosity have been preferentially used to culture the cells to achieve better optical clarity and cell adhesions. However, these membranes limit intercellular communications between cells on each side of

the membrane because of sparse through-holes and small open areas.

After confirming that the type I collagen could act as a scaffold by blocking pores of the porous membrane, we compared the commonly used PETE membranes of 1, 5, and 10 μm-pore sizes to verify that the membrane with the large pore is optically advantageous over other membrane options. For the comparison, we first measured the effective PSFs that are obtained after the light path is aberrated passing through the PETE membranes (figure 2(a)). We then simulated predicted fluorescence images based on the measured PSFs of the PETE membranes with different pore sizes and pore densities. By applying convolution of an aberration free image of cells taken under membrane-free conditions with the aberrated PSFs due to the PETE membranes, we visualized artificial images of the cultured cells on each membrane (figure 2(b)). The quality of each aberrated image was then compared to the ground truth image by using the SSIM [21]. SSIM values range from 0 to 1, where 1 corresponds to a perfect match between the ground truth and aberrated images. For the images aberrated by low pore density 1 μm-pore and 10 μm-pore PETE membranes, SSIM values were 0.95 and 0.96. However, at high pore density 1 μm-pore and 5 μm-pore PETE membranes, SSIM values dropped to 0.74 and 0.86 (figure S3). These results reflect that the low pore density membrane or large pore size membrane are more optically transparent and offer superior image quality closer to the membrane-free condition. Next, the simulated images were compared with actual images of cultured cells (GFP-HUVECs) on the cECMTE membrane (figure 2(c)). Comparing each image revealed that the effects of condensed ECM on the optical transparency of each membrane were minimal, and the transparency of the cECMTE membrane continues to vary depending on the density and size of the pores. As shown in figures 2(b) and (c), when the membrane pore size increased, or the density of the pores decreased, the optical properties were improved with reduced background haze and clearer cell visibility.

To visualize the 3D MPS constructed in a microfluidic device, the z-stacking feature of a confocal microscope was utilized for slicing and integrating images along the *z*-axis of the MPS device (figure 2(d)). As shown in the reconstructed 3D image, the cell monolayers in the upper (GFP-HUVEC, green) and lower (A549, red) sides of the low pore density 1 μm-pore PETE membrane (figure 2(d) left) and 10 μm-pore PETE membrane (figure 2(d) right) were visually distinguishable while they were not optically partitionable due to the intense light scattering through the high pore density 1 μm-pore PETE membrane (figure 2(d) middle).

Figure 2. Optical properties of different pore-sized PETE membranes. (a) PSF of PETE membranes with different porosity and pore sizes. Scale bar = 5 μm. (b) Convoluted images of the obtained PSF by applying to the reference GFP-HUVEC image taken without a membrane condition. Scale bar = 100 μm. (c) The actual images of GFP-HUVECs cultured on each cECMTE membrane. Scale bar = 100 μm. (d) Representative 3D coculture images of GFP-HUVECs and CellTracker Red-stained A549 on the different pore-sized PETE membranes.

Overall, while both the low pore density 1 and the 10 μm-pore PETE membrane resulted in comparable outstanding optical transparency, the larger pore membrane is predicted to be more advantageous in creating MPS because of the facilitated cellular interactions and transmigration of cells across the membrane.

3.3. BBB reconstruction and characterization on a cECMTE membrane in an MPS device

We next explored the application of the PMMA MPS device in the reconstitution of human BBB. The

BBB functions as a specialized physiological barrier to protect the central nervous system by restricting the entry of unwanted molecules from the blood into the brain. This restrictive interface formed by hBMECs limits the paracellular permeability and actively pump out a massive variety of lipophilic drugs through efflux transporters on the membrane. While hBMECs form the main interface, they work in concert with glial cells, including astrocytes that surround tissue space extending their processes toward the endothelium. They adapt to environmental changes and regulate the functional maintenance of BBB
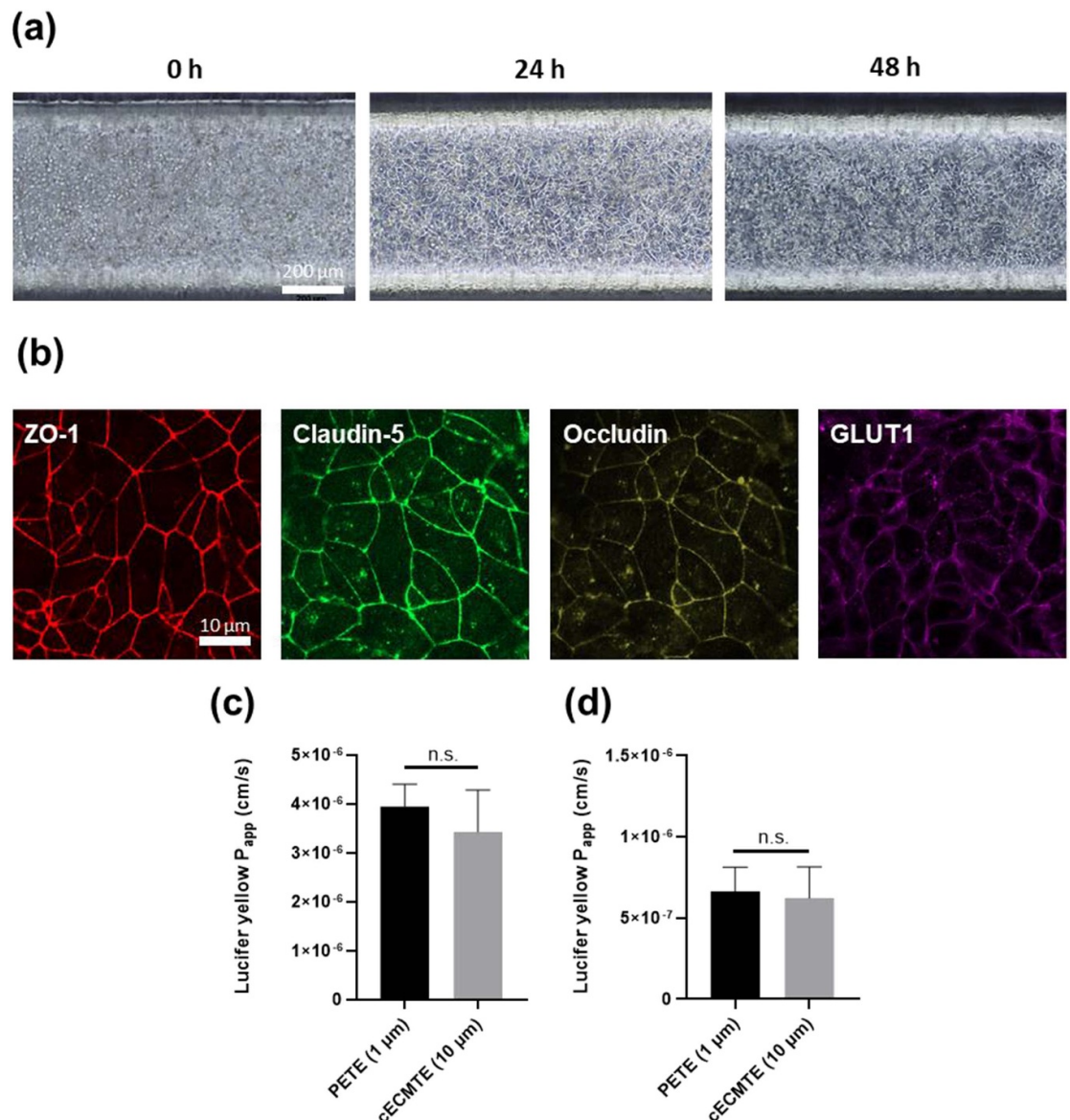
Figure 3. Characterization of the BBB on the 10 μm-pore cECMTE membrane in the MPS device. (a) Bright field images showing the morphology of hBMECs seeded on a 10 μm-pore cECMTE membrane. Scale bar = 200 μm. (b) Immunofluorescence images of the hBMECs cultured on the device for 2 d stained with ZO-1, claudin5, occludin, and GLUT1. Scale bar = 10 μm. (c) The apparent permeability of Lucifer yellow across the bare 1 μm-pore PETE membrane and the 10 μm-pore cECMTE membrane in the empty MPSs without a cell monolayer. (d) The apparent permeability of Lucifer yellow across the hBMECs monolayers on the 1 μm-pore PETE membrane without condensed ECM and the 10 μm-pore cECMTE membrane in the BBB MPSs. The results are presented as the mean ± s.e.m. performed in triplicate. For statistical analysis, an unpaired t-test was performed (n.s., not significant).

together through dynamic cell-to-cell communications [22–24]. Thus, multicellular BBB models have found increasing applications to study molecular mechanisms underlying tumor cells or drug permeability across the dynamic interface.

In general, PETE membranes with a small pore size (0.4 ~ 2 μm) are used for culturing iPSC-derived hBMECs [6] because PETE membranes with large pores (>5 μm) are not able to support the stable attachment of hBMECs on the substrate due to the low contact area [10]. However, the use of a small pore-sized membrane limited the application range of the BBB model.

We set out to generate a human BBB monolayer on a 10 μm-pore cECMTE membrane in the PMMA MPS device. Human iPSC-derived BMECs were seeded on the cECMTE membrane in the upper microchannel with different cell densities. The endothelial monolayer was successfully formed within 24 h when hBMECs were seeded at a density of 1.2×10^7 cells ml^{-1} (figure 3(a)). However, hBMECs plated at a higher density (1.7×10^7 cells ml^{-1}) showed low cell attachments because of nutritional and oxygen deficiency (data not shown). The cells were not observed in the lower channel since the condensed ECM provided enough contact

area, preventing hBMECs from passing through the 10 μm-pores. After 2 d of hBMECs culture, confocal immunofluorescence microscopic analysis revealed the tight junctional integrity of the BBB, showing the localization of tight junction proteins, including ZO-1, claudin-5, and occludin, at the endothelial border (figure 3(b)). It also showed the expression of GLUT1, which is responsible for glucose transport across the BBB (figure 3(b)).

The barrier integrity of the BBB was examined by analyzing the paracellular transport of Lucifer yellow (457.3 g mol^{-1}) in the BBB MPS (figures 3(c) and (d)). To compare with a previous method, the BBB integrity was measured in two types of the MPS devices assembled with different membranes—the PETE membrane with small pores (1 μm) without condensed ECM as a positive control and the 10 μm-pore cECMTE membrane. The insignificant difference in the permeability between the two types of membranes was determined in the empty MPS devices without a cell monolayer (figure 3(c)). As shown in figure 3(d), the apparent permeability of Lucifer yellow across the BBB monolayer on the cECMTE membrane was comparable to those obtained from the BBB culture on the PETE (1 μm) membrane, implying that the reconstructed BBB on cECMTE offers physical barriers as strong as the conventional BBB culture on the 1 μm-pore PETE membrane effectively limiting the paracellular diffusion.

3.4. A highly permeable cECMTE membrane facilitates physical contact between brain endothelial cells and astrocytes, leading to the maturation of BBB

It is generally accepted that commercially available small pore-sized PETE membranes (0.4 $\sim$ 2 μm) with high transparency allow only chemical communications between hBMECs and astrocytes [25, 26]. We hypothesized that a large pore-sized (10 μm) cECMTE membrane would promote the astrocytes to interact with the brain endothelial layer with their endfeet by extending the processes through the pores, reproducing a more *in vivo*-like phenotype (figure 4(a)). To reconstitute the multicellular BBB in the MPS device, human primary astrocytes were seeded in the lower channel and incubated for 2 h after flipping the device to allow the cells to be attached on the membrane. A confocal microscopic image from the side view revealed that astrocytic processes are in close contact with hBMECs by penetrating the cECMTE membrane (figure 4(b) and video 1). A confocal image taken at the lower side of the membrane showed that some processes of astrocytes sent out projections toward a pore (figure 4(c), bottom panel) and terminated in
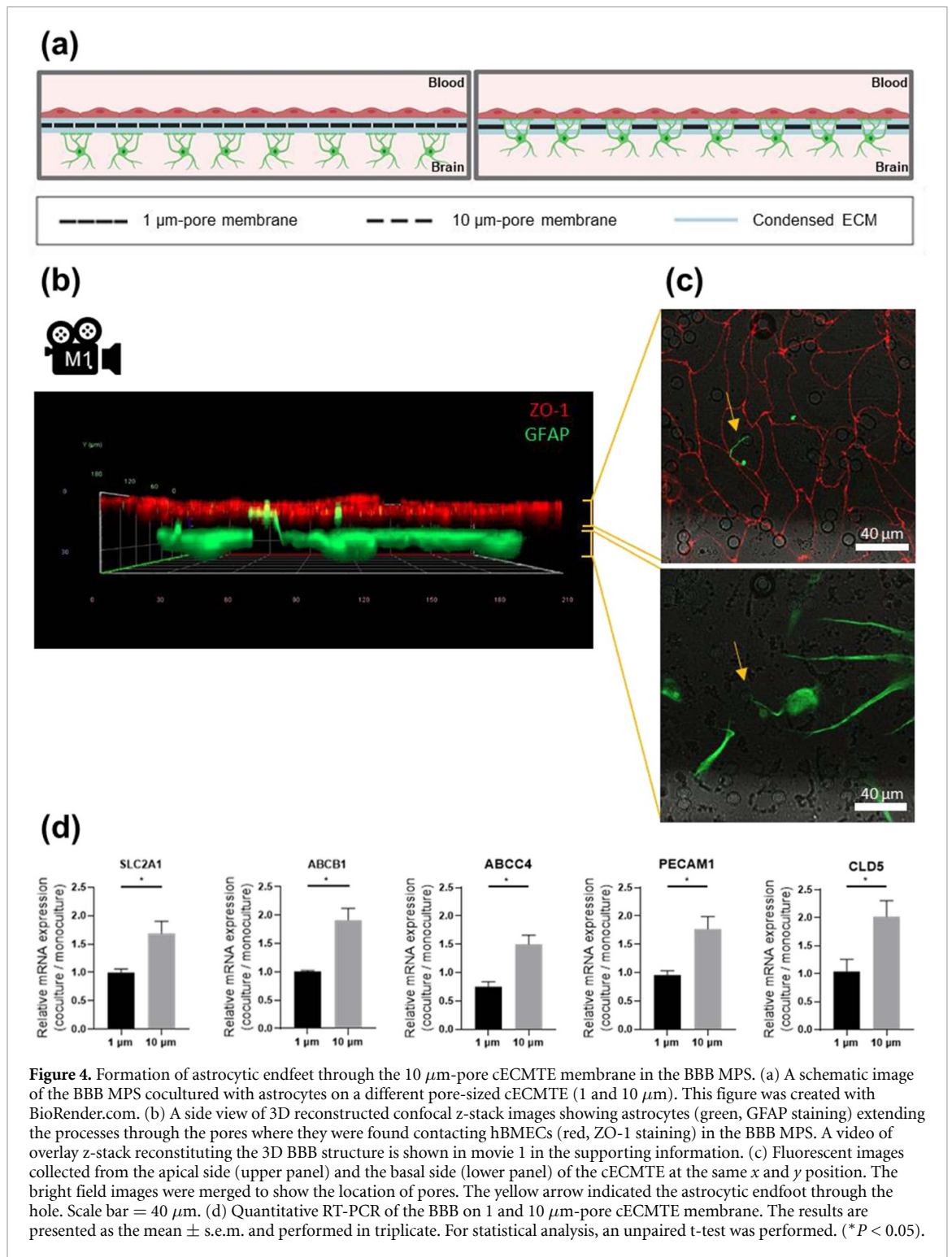
prolongation localized with hBMECs (figure 4(c), upper panel), forming the 3D structure of astrocytic endfeet.

Next, we analyzed mRNA expressions of the BBB functional genes in iPSC-derived hBMECs, which are known to be enhanced by coculture with astrocytes [27]. The mRNA expressions were compared between hBMECs monoculture and coculture on each type of membranes to test if these different pore-sized membranes (1 and 10 μm) sufficiently support the interplay between hBMECs and astrocytes. As shown in figure 4(d), when hBMECs were cocultured with astrocytes on the 10 μm-pore cECMTE membrane, mRNA expressions of glucose transporter protein (SLC2A1), drug efflux pump protein (ABCB1, ABCC4), tight junction protein (CLD5), and endothelial junction (PECAM-1) were increased by 1.5 $\sim$ 2-fold compared to those in the monoculture condition. In contrast, when hBMECs were cocultured with astrocyte on the 1 μm-pore cECMTE membrane in the same device, mRNA expressions were not markedly changed due to physical obstruction of small pores. However, the barrier integrity of the monolayer of hBMECs coculture was not apparently changed by co-culture with astrocytes in the BBB MPSs (figure S4). These studies revealed that hBMECs-astrocytes interaction may have been more facilitated in the large pore-sized membrane via the formation of astrocytic endfeet and better exchange of secreted factors through the larger open area (>5 times) of the 10 μm-pore PETE membrane.

3.5. 10 μm-pore cECMTE membranes permit transendothelial migration on the BBB MPS

To further investigate the potential of the BBB MPS as an *in vitro* platform to study tumor metastasis, we investigated the transmigration of two different human breast tumor cells, MCF-7 and MDA-MB-231, in the BBB MPS. Our BBB MPS was assumed to provide a through-hole diameter (10 μm) large enough for tumor cells to migrate across the BBB while the past *in vitro* BBB models using small pore-sized membranes (0.4 $\sim$ 2 μm) did not sufficiently allow the tumor cell migration through pores (figure 5(a)). To monitor the adhesion and extravasation of metastatic tumor cells (MDA-MB-231) and non-metastatic tumor cells (MCF-7) in the BBB, both types of cells were labeled with CellTracker Green and introduced to the upper channel of the BBB MPS. We compared the number of cells adhered to hBMECs between MDA-MB-231 and MCF-7 to ensure that they were responding to endothelium depending on their aggressiveness. In the BBB MPS, highly metastatic MDA-MB-231 adhered to hBMECs three times more than MCF-7 at 24 h after the tumor

Figure 4. Formation of astrocytic endfeet through the 10 μm-pore cECMTE membrane in the BBB MPS. (a) A schematic image of the BBB MPS cocultured with astrocytes on a different pore-sized cECMTE (1 and 10 μm). This figure was created with BioRender.com. (b) A side view of 3D reconstructed confocal z-stack images showing astrocytes (green, GFAP staining) extending the processes through the pores where they were found contacting hBMECs (red, ZO-1 staining) in the BBB MPS. A video of overlay z-stack reconstituting the 3D BBB structure is shown in movie 1 in the supporting information. (c) Fluorescent images collected from the apical side (upper panel) and the basal side (lower panel) of the cECMTE at the same *x* and *y* position. The bright field images were merged to show the location of pores. The yellow arrow indicated the astrocytic endfoot through the hole. Scale bar = 40 μm. (d) Quantitative RT-PCR of the BBB on 1 and 10 μm-pore cECMTE membrane. The results are presented as the mean $\pm$ s.e.m. and performed in triplicate. For statistical analysis, an unpaired t-test was performed. (*$P < 0.05$).
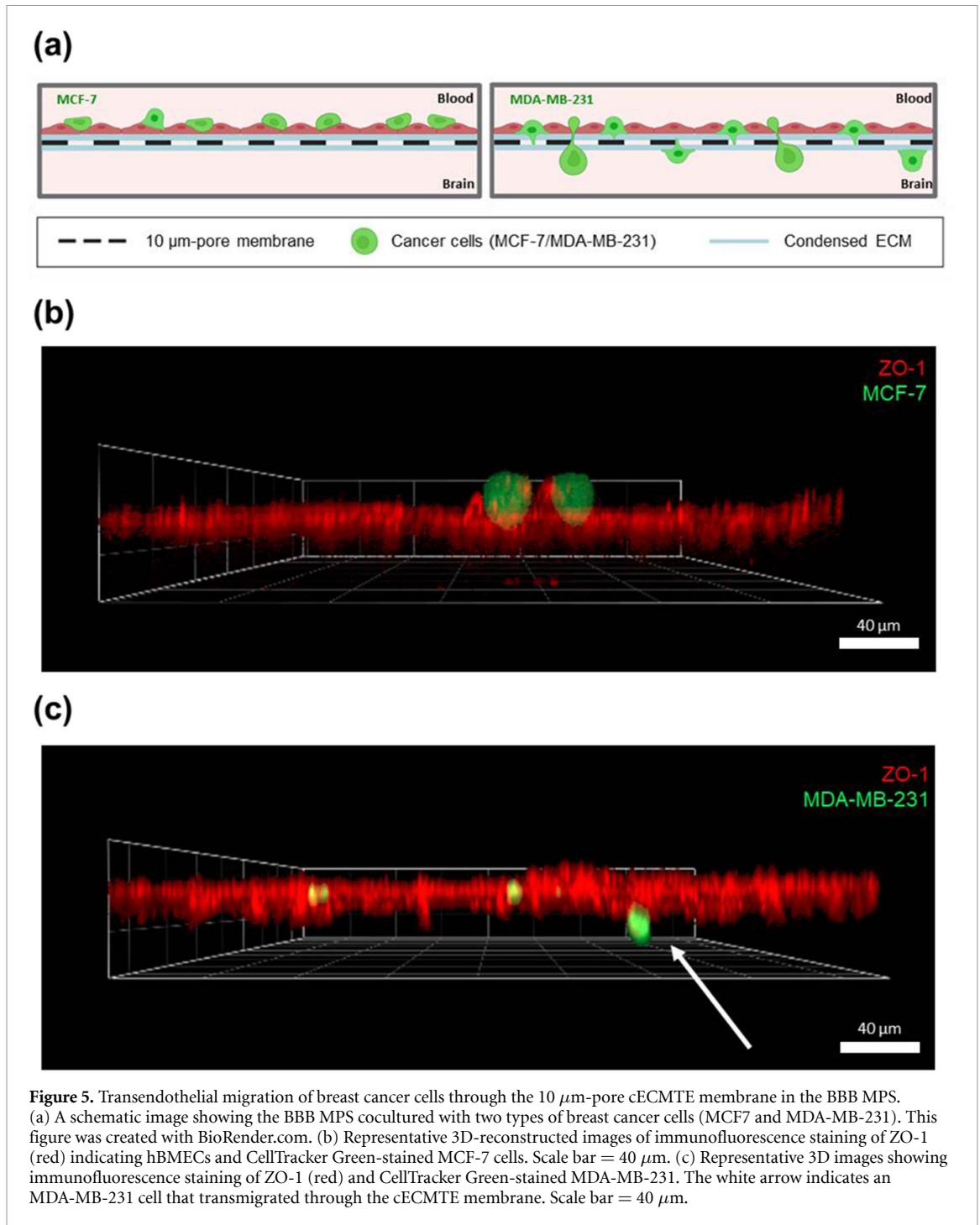
cells were introduced, which was consistent with previous studies (figure S5) [28, 29]. The extravasation event was observed using confocal microscopy at the surface and cross-sectional views. As shown in figures 5(b) and S6, MCF-7 cells labeled with a green dye were found only on the apical side of hBMECs, denoted by ZO-1 staining in red. In contrast, MDA-MB-231 cells were captured at the lower channel where they have transmigrated across the BBB (figures 5(c) and S6). Together, these results support that the 10 μm-pore cECMTE membrane in the MPS device can recapitulate the dynamic interaction of the BBB with tumor cells with different invasive potential and enable a well-visualized study of tumor extravasation in the brain (figures 5(b), (c) and S6).

Figure 5. Transendothelial migration of breast cancer cells through the 10 μm-pore cECMTE membrane in the BBB MPS. (a) A schematic image showing the BBB MPS cocultured with two types of breast cancer cells (MCF7 and MDA-MB-231). This figure was created with BioRender.com. (b) Representative 3D-reconstructed images of immunofluorescence staining of ZO-1 (red) indicating hBMECs and CellTracker Green-stained MCF-7 cells. Scale bar $= 40$ μm. (c) Representative 3D images showing immunofluorescence staining of ZO-1 (red) and CellTracker Green-stained MDA-MB-231. The white arrow indicates an MDA-MB-231 cell that transmigrated through the cECMTE membrane. Scale bar $= 40$ μm.

4. Conclusions

Fabrication of microphysiological barriers has been a daunting challenge because mimicking their structural and functional characteristics is often limited by fabrication techniques, such as a resolution of bioprinting and photolithography. Although TE membranes have been employed to construct a tissue barrier interface in an MPS due to their simplicity, there have been challenges, such as limited transmigration through a small pore-sized membrane, poor adhesion of cells to the surface of a membrane with large pore size, and optical translucence due to light scattering through pores. Despite considerable efforts in recent years, no fabrication approach was developed, which could address these problems simultaneously. This is an important problem as it is necessary for the cells on both sides of the porous membranes to freely interact with their neighboring cells and transmigrate through the barriers without physical restriction because these confinements of the cells could potentially mislead experimental results obtained from the MPS platform.

Our approach offers the unique capability in addressing all unmet needs in fabricating the adjustable ECM-layered membrane integrated with

an MPS. Due to the various extracellular features in the tissue-specific microenvironment, it is also critical to adjust ECM thickness and their compositions. We demonstrated that the height of the fibrous ECM films deposited on the TE membranes could be determined by the concentration of ECM proteins in a solution. This feature also could be accomplished by changing the height of the microfluidic channel because the channel volume determines the amount of ECM proteins to be condensed on the surface. Moreover, a mixture of a range of ECM proteins, such as type I collagen, type IV collagen, fibronectin, and Matrigel, can be used to form cECMTE membranes once they are gelated in the microfluidic channel, and additional coating with other ECM proteins on top of the cECMTE surface is also practicable. Although we validated our method using a 10 μm-pore size PETE membrane, we could extend this to other types of porous membranes of different materials, such as PC, polyimide, and PDMS. In addition, TE membranes with pore sizes larger than 10 μm could be applicable depending on the requirement of membrane permeability; however, we set out to examine the 10 μm-pore TE membrane because it permitted large pores enough for the cells to communicate and translocate across the membrane. Given the diverse chip configurations and fabrication process of commercial MPS platforms or those on the way to the market, our method could provide a versatile utility in providing an adjustable ECM microenvironment of tissue-specific barrier interfaces in an organ-mimicking *in vitro* analytical platform.

Data availability statement

All data that support the findings of this study are included within the article (and any supplementary files).

Acknowledgments

Notes

The authors declare no competing financial interest.

Author contributions

The manuscript was written through contributions of all authors. All authors have given approval to the final version of the manuscript.

ORCID iDs

Brian Choi ⓘ https://orcid.org/0000-0001-9012-475X
Jeong-Won Choi ⓘ https://orcid.org/0000-0001-8287-450X
Tae-Eun Park ⓘ https://orcid.org/0000-0003-3979-5405
Joo H Kang ⓘ https://orcid.org/0000-0001-9636-3209

References

[1] Zhang B, Korolj A, Lai B F L and Radisic M 2018 Advances in organ-on-a-chip engineering *Nat. Rev. Mater.* **3** 257–78

[2] Sung J H, Koo J and Shuler M L 2019 Mimicking the human physiology with microphysiological systems (MPS) *Biochip J.* **13** 115–26

[3] Perry G, Xiao W, Welsh G I, Perriman A W and Lennon R 2018 Engineered basement membranes: from *in vivo* considerations to cell-based assays *Int. J. Integr. Biol.* **10** 680–95

[4] van Meer B, de Vries H, Firth K, van Weerd J, Tertoolen L, Karperien H, Jonkheijm P, Denning C, IJzerman A and Mummery C 2017 Small molecule absorption by PDMS in the context of drug response bioassays *Biochem. Biophys. Res. Commnun.* **482** 323–8

[5] Chung H H, Mireles M, Kwarta B J and Gaborski T R 2018 Use of porous membranes in tissue barrier and co-culture models *Lab Chip* **18** 1671–89

[6] Park T-E, Mustafaoglu N, Herland A, Hasselkus R, Mannix R, FitzGerald E A, Prantil-Baun R, Watters A, Henry O and Benz M 2019 Hypoxia-enhanced blood-brain barrier chip recapitulates human barrier function and shuttling of drugs and antibodies *Nat. Commun.* **10** 2621–32

[7] Jang K-J, Mehr A P, Hamilton G A, McPartlin L A, Chung S, Suh K-Y and Ingber D E 2013 Human kidney proximal tubule-on-a-chip for drug transport and nephrotoxicity assessment *Int. J. Integr. Biol.* **5** 1119–29

[8] Ferraz M A M M *et al* 2018 An oviduct-on-a-chip provides an enhanced *in vitro* environment for zygote genome reprogramming *Nat. Commun.* **9** 4934–47

[9] Vandenhaute E, Drolez A, Sevin E, Gosselet F, Mysiorek C and Dehouck M-P 2016 Adapting coculture *in vitro* models of the blood–brain barrier for use in cancer research: maintaining an appropriate endothelial monolayer for the assessment of transendothelial migration *Lab. Invest.* **96** 588–98

[10] Casillo S M, Peredo A P, Perry S J, Chung H H and Gaborski T R 2017 Membrane pore spacing can modulate endothelial cell–substrate and cell–cell interactions *ACS Biomater. Sci. Eng.* **3** 243–8

[11] Mondrinos M J, Yi Y-S, Wu N-K, Ding X and Huh D 2017 Native extracellular matrix-derived semipermeable, optically transparent, and inexpensive membrane inserts for microfluidic cell culture *Lab Chip* **17** 3146–58

[12] Nguyen T, Jung S H, Lee M S, Park T-E, Ahn S-K and Kang J H 2019 Robust chemical bonding of PMMA microfluidic devices to porous PETE membranes for reliable cytotoxicity testing of drugs *Lab Chip* **19** 3706–13

[13] Peppas N A, Hilt J Z, Khademhosseini A and Langer R 2006 Hydrogels in biology and medicine: from molecular principles to bionanotechnology *Adv. Mater.* **18** 1345–60

[14] Wallace D G and Rosenblatt J 2003 Collagen gel systems for sustained delivery and tissue engineering *Adv. Drug Deliv. Rev.* **55** 1631–49

[15] Gross J and Kirk D 1958 The heat precipitation of collagen from neutral salt solutions: some rate-regulating factors *J. Biol. Chem.* **233** 355–60

[16] Kadler K E, Holmes D F, Trotter J A and Chapman J A 1996 Collagen fibril formation *Biochem. J.* **316** 1–11

[17] Puleo C M, Ambrose W M, Takezawa T, Elisseeff J and Wang T-H 2009 Integration and application of vitrified collagen in multilayered microfluidic devices for corneal microtissue culture *Lab Chip* **9** 3221–7

[18] Takezawa T, Takeuchi T, Nitani A, Takayama Y, Kino-Oka M, Taya M and Enosawa S 2007 Collagen vitrigel membrane useful for paracrine assays *in vitro* and drug delivery systems *in vivo J. Biotechnol.* **131** 76–83

[19] Takezawa T, Ozaki K, Nitani A, Takabayashi C and Shimo-Oka T 2004 Collagen vitrigel: a novel scaffold that can facilitate a three-dimensional culture for reconstructing organoids *Cell Transplant.* **13** 463–74

[20] Sellgren K L, Hawkins B T and Grego S 2015 An optically transparent membrane supports shear stress studies in a three-dimensional microfluidic neurovascular unit model *Biomicrofluidics* **9** 061102

[21] Wang Z, Bovik A C, Sheikh H R and Simoncelli E P 2004 Image quality assessment: from error visibility to structural similarity *IEEE Trans. Image Process.* **13** 600–12

[22] Abbott N J 2002 Astrocyte–endothelial interactions and blood–brain barrier permeability *J. Anat.* **200** 523–34

[23] Kubotera H, Ikeshima-Kataoka H, Hatashita Y, Mascaro A L A, Pavone F S and Inoue T 2019 Astrocytic endfeet re-cover blood vessels after removal by laser ablation *Sci. Rep.* **9** 1263–72

[24] Demeuse P, Kerkhofs A, Struys-Ponsar C, Knoops B, Remacle C and de Aguilar P V D B 2002 Compartmentalized coculture of rat brain endothelial cells and astrocytes: a syngenic model to study the blood–brain barrier *J. Neurosci. Methods* **121** 21–31

[25] He Y, Yao Y, Tsirka S E and Cao Y 2014 Cell-culture models of the blood–brain barrier *Stroke* **45** 2514–26

[26] Booth R and Kim H 2012 Characterization of a microfluidic *in vitro* model of the blood-brain barrier (μBBB) *Lab Chip* **12** 1784–92

[27] Goldeman C, Ozgür B and Brodin B 2020 Culture-induced changes in mRNA expression levels of efflux and SLC-transporters in brain endothelial cells *Fluids Barriers CNS* **17** 32–43

[28] Drolez A, Vandenhaute E, Julien S, Gosselet F, Burchell J, Cecchelli R, Delannoy P, Dehouck M-P and Mysiorek C 2016 Selection of a relevant *in vitro* blood-brain barrier model to investigate pro-metastatic features of human breast cancer cell lines *PLoS One* **11** e0151155

[29] Spencer A, Spruell C, Nandi S, Wong M, Creixell M and Baker A 2016 A high-throughput mechanofluidic screening platform for investigating tumor cell adhesion during metastasis *Lab Chip* **16** 142–52